INTERNATIONAL JOURNAL FOR NUMERICAL METHODS IN FLUIDS
Int. J. Numer. Meth. Fluids 2008; **57**:1005–1021
Published online 27 November 2007 in Wiley InterScience (www.interscience.wiley.com). DOI: 10.1002/fld.1670

Interference effect of two equal-sized square cylinders in tandem arrangement: With planar shear flow

A. Lankadasu[§] and S. Vengadesan[*, †, ‡]

Department of Applied Mechanics, IIT Madras, Chennai-36, India

SUMMARY

Numerical simulations have been performed for flow past two equal-sized square cylinders in tandem arrangement subjected to incoming planar shear flow. Effect of L/d ratio and the shear parameter has been studied. The range of L/d ratio (ratio of center-to-center distance (L) to cylinder width (d)) is varied from 2 to 7 and the non-dimensional shear parameter (K) is varied from 0.0 to 0.4 in steps of 0.1. For all the cases the Reynolds number (Re) based on centerline velocity and cylinder width is fixed at 100. The results are compared with that of isolated square cylinder with uniform flow. Strouhal number decreases with increasing shear parameter. There are more than one shedding frequency at high shear parameters and L/d ratios. The mean drag coefficient is decreased with shear parameter and lesser than that of the single cylinder. The root mean square (RMS) value of both lift and drag coefficients is higher for the downstream cylinder for all values of shear parameter. With increasing L/d ratio, for both lift and drag, the RMS value increases and then decreases for upstream cylinder, whereas it continuously increases for the downstream cylinder. The stagnation point is moved towards the top leading edge with increasing shear. The critical L/d ratio, which is defined as the distance between two cylinders, beyond which the vortex shedding from the upstream cylinder occurs, decreases with increasing shear parameter.

Received 29 January 2007; Accepted 15 October 2007

KEY WORDS: shear parameter; tandem arrangement; square cylinders; laminar vortex shedding; incompressible flow; two-dimensional

1. INTRODUCTION

There has been great improvement in the understanding of bluff body wake in the last few decades. Extensive experimental and numerical studies have been reported with new insights. However, most of the works concentrated on isolated circular cylinder with uniform free-stream flow. However,

*Correspondence to: S. Vengadesan, Department of Applied Mechanics, IIT Madras, Chennai-36, India.
†E-mail: vengades@iitm.ac.in
‡Assistant Professor.
§Research Scholar.

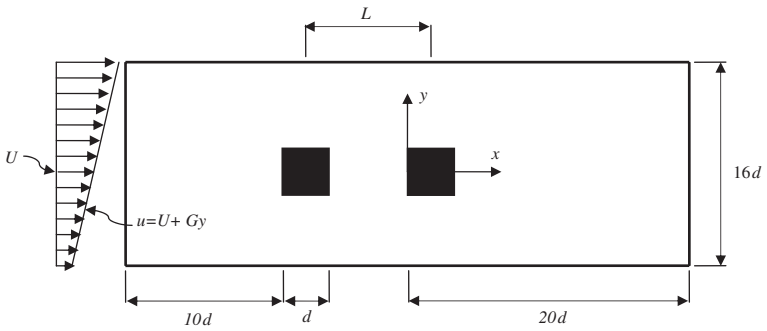

Figure 1. Computational domain and coordinate system.

when the incoming flow has turbulence or shear (embedded vorticity) or interference affects, the wake flow becomes different from that of uniform flow [1–5]. Further, these effects are different for different types of cylinders, like circular, square, rectangular, etc. The main distinction between smooth-edged and sharp-edged cylinders is the point of separation. In the case of the former one, the separation point is not fixed, whereas in latter one, it is fixed. This alters the flow dynamics considerably.

When more than one bluff body is placed in a fluid flow, the resulting forces and vortex shedding pattern may be completely different from those forces on a single body at the same Reynolds number [6, 7]. Among the many possible arrangements in which two square cylinders can be positioned relative to a cross-flow, the tandem arrangement is one type and it is shown in Figure 1. In this arrangement, the type of interference present is wake interference, where the wake of the upstream cylinder affects the flow past the downstream one. The effect of this interference is seen, for example, in the variation of the Strouhal number (St) and force coefficients as a function of the center-to-center distance (L/d). Many of the previous studies regarding the flow around two circular cylinders and square cylinders identified diverse interference regimes [5, 7–11]. The classification proposed by Sakamoto *et al.* [8] for square cylinders in tandem arrangement is adopted in this study. According to this classification, three different interference regimes can be identified: (1) a regime where vortices are shed from the downstream cylinder alone; (2) a regime where the vortices shed from the downstream cylinder synchronize with the ones from the upstream cylinder and (3) a regime where the vortices are shed individually from each body.

In practice many structures, such as offshore structures, pipe lines near the seabed, are immersed in a boundary layer. When a small cylinder is placed in the boundary layer of a large main cylinder to alter the vortex shedding phenomena behind the main cylinder, the small cylinder is inevitably subjected to the effect of shear induced from the large cylinder. These are typical cases with non-uniform approach flows. The simplest case of a non-uniform flow for the investigation of the velocity gradient effect is the uniform shear flow, which has a linear distribution of the longitudinal velocity component along the transverse direction. It has been shown by past investigations on circular cylinders, e.g. [12–17], that the flow approaching with linear shear has greatly altered the vortex dynamics in the wake when compared with that in the uniform flow case. They attributed this to the constant vorticity embedded in the free stream. However, much less work is reported on the square cylindrical bodies, e.g. [2, 3, 18–21]. Ayukawa *et al.* [18] conducted experiments and

DOI: 10.1002/fld

performed discrete vortex simulations at Reynolds number $Re=4000$, and observed that with high shear parameters the flow becomes self-similar downstream of the cylinder. Saha *et al.* [20, 21] studied the same problem numerically for a wide range of Reynolds numbers. They showed that due to the influence of shear, the Karman vortex street mainly consists of clockwise vortices, whose decay is very slow when compared with that in the uniform flow. However, in their study the lateral width, W, of the flow domain was restricted such that the streamwise velocity in the free stream was constantly positive ($u>0$), that is, the free stream could not flow in the reverse direction due to the imposed shear rate. In other words, the study is limited to low shear parameters and with high blockage ratio. Recently, Cheng *et al.* [2, 3] have reported that vortex shedding disappeared for large shear parameters. Both the Strouhal number and the drag coefficient decrease with increasing shear parameter.

However, there is no reference available in the open literature on shear flow over a pair of square cylinders in tandem arrangement. The objective of the present 2-D numerical simulations is to study the effect of linear shear flow over a two equal square cylinders in tandem arrangement. The range of shear parameter is varied from 0.0 to 0.4 in steps of 0.1 and center-to-center distance is varied from 2 to 7. The Reynolds number based on cylinder width and centerline velocity is fixed at 100. At this *Re*, the flow behavior is 2D and laminar.

2. PHYSICAL AND MATHEMATICAL FORMULATION

The flow under consideration in this study is 2-D, unsteady, viscous and incompressible with constant fluid properties around a pair of equal-sized square cylinders. The cylinders are placed in tandem arrangement subjected to uniform shear flow. For this laminar flow, the equations for continuity and momentum in non-dimensional form are expressed as

$$\frac{\partial u_i}{\partial x_i}=0 \tag{1}$$

$$\frac{\partial u_i}{\partial t}+u_j\frac{\partial u_i}{\partial x_j}=-\frac{\partial p}{\partial x_i}+\frac{1}{Re}\frac{\partial^2 u_i}{\partial x_j\partial x_j} \tag{2}$$

where indices i, $j=1,2$ refer to the streamwise (x), and cross-stream (y) directions of the Cartesian coordinate system, respectively. All geometrical lengths are normalized with cylinder width d, velocities with the speed of the undisturbed flow at the center of the upstream cylinder U, physical times with d/U and pressure with the dynamic pressure ρU^2.

Figure 1 shows the computational domain. The flow is described in a Cartesian coordinating system (x and y) in which the x-axis is aligned with the inlet flow direction (streamwise direction) and the y-axis is normal to the x-axis (cross-stream direction). The origin is positioned at the midpoint of the upstream face of the downstream cylinder. The first grid point from the body is maintained at 0.008 times the cylinder width (d). For getting better predictions, the number of points on each face of the cylinder is fixed at 50. To adjust these points on the entire face, we followed the non-uniform distribution of nodes on the each face of the cylinder. At the corners, we maintained minimum distance and then uniformly stretched up to the center of the face from both the corners [22]. The grid in the region between the cylinders is stretched up to $0.5d$ from both cylinders and then maintained uniform for the remaining gap. The grid distribution in the rest of

DOI: 10.1002/fld

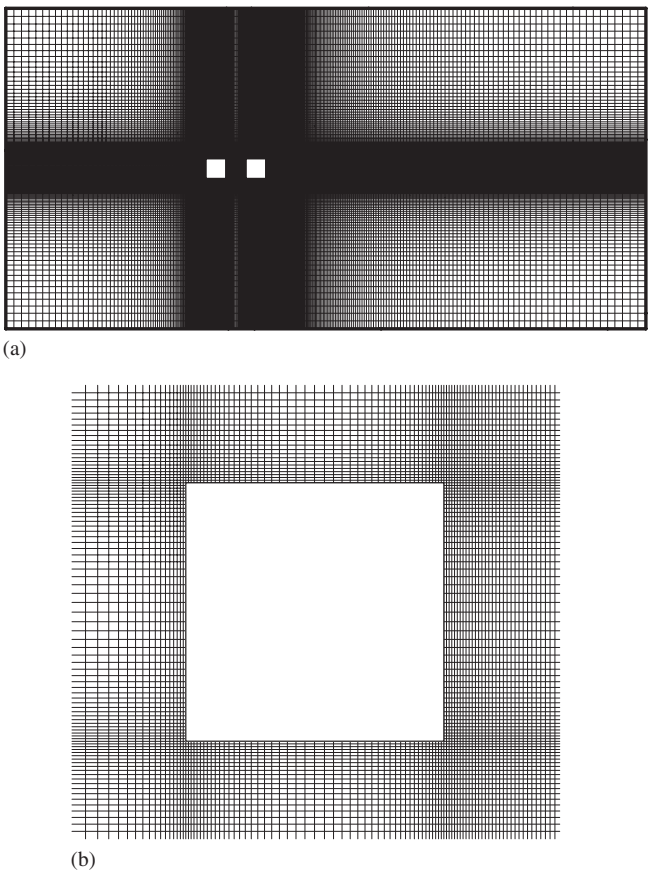

Figure 2. The grid used for gap ratio $L/d=2$: (a) full domain and (b) grid in the vicinity of cylinder.

the domain both in streamwise and cross-stream directions was made non-uniform with constant stretching ratio. The grid used for $L/d=2$ case is illustrated in Figure 2.

3. NUMERICAL DETAILS

A finite-difference code with staggered grid arrangement in which velocity components are defined at the midpoint of the cell face to which they are normal and pressure is at the center of the cell is used. After discretization, Equations (1) and (2) were solved with an explicit method. A third-order upwind-biased scheme for convective terms, central differencing scheme for diffusion terms and a second-order accurate Adams–Bashforth scheme for time marching were used. Time marching was done in two stages. In the first stage, two velocity components are calculated using previous values of velocities and pressure for all the cells. However, these values do not necessarily satisfy the mass conservation criteria imposed by the continuity equation (i.e. divergence-free condition for incompressible flow). Thus in the second stage, adjustment must be made to ensure mass

DOI: 10.1002/fld

Table I. Comparison of isolated square cylinder with uniform flow ($K=0.0$): root mean square value of lift coefficient, Strouhal number and mean coefficient of drag results with simulations and experiments at $Re=100$ and also for $K=0.1, 0.2, 0.3$ and 0.4.

Author	K	$C_{L,rms}$	St_0	$\overline{C}_{D,0}$
Okajima [28]	0.0		0.140	—
Sohankar *et al.* [22]	0.0	0.156	0.146	1.46
Cheng *et al.* [2]	0.0	0.152	0.145	1.44
Present calculations (260×220)	0.0	0.157	0.143	1.47
Present calculations (226×195)	0.0	0.159	0.143	1.47
	0.1		0.143	1.46
	0.2		0.114	1.45
	0.3		0.045	0.90
	0.4		0.045	0.68

conservation. This is done by using the Highly Simplified Marker and Cell algorithm [23]. Basic validation of the code can be found in References [24, 25].

The time marching calculations were started with the fluid at rest. A constant non-dimensional time step $\Delta t=0.0005$ was used for all the calculations. The conditions necessary to prevent the numerical oscillations are determined from the Courant–Freidrichs–Lewy condition and the restriction on the grid Fourier number. In this study, a convergence limit of 0.0005 was typically used.

At the inlet, a linear velocity profile ($u=U+Gy, v=0$) was assumed, where U is the centerline velocity and G is the shear gradient, which is normalized as $K=Gd/U$. For high G values and beyond a certain blockage ratio, u is negative on the lower velocity side [26]. At the outlet boundary, the convective boundary condition ($\partial u_i/\partial t+U_c(\partial u_i/\partial x_j)=0$) was used for both velocity components. No-slip conditions were prescribed at the body surface. At the top and bottom boundaries, in this work, we have used $\partial u/\partial y=K, v=0$. It should be noted that, if the K value is zero, this condition results in symmetry condition, which is the most commonly used far-field boundary condition.

The numerical scheme as explained above is validated for the case of incoming linear shear flow past an isolated square cylinder [27]. Results are compared in Table I. For the present 2-D computations, two grids of size 260×220 and 226×195 have been considered. Table I shows the computed root mean square (RMS) value of lift coefficient ($C_{L,rms}$), mean coefficient of drag ($\overline{C}_{D,0}$) and Strouhal number (St_0), which is defined using the vortex shedding frequency (f), cylinder width (d) and the centerline velocity (U). The variation of $C_{L,rms}$, $\overline{C}_{D,0}$ and St_0 between two grids is almost negligible. For the case of uniform approach flow, computed results are compared with the available literature and found to be in good agreement.

To verify the results for interference cases on grid resolution, two grids of the same stretching parameter and first grid point as the isolated square cylinder have been used. We obtained 469×220 and 437×195 grid points for the $L/d=5$ case. This case is the most representative of all the remaining cases. Using these grids, we computed two situations *viz.* no shear ($K=0.0$) and maximum shear ($K=0.4$). For these calculations, we compared bulk parameters with each other in Table II and found insignificant difference between the results of these two grids. Hence, we have taken parameters of the grid 437×195 to arrive at the grid for the rest of the simulations. Please note that depending on the L/d ratio, the number of grid points in the streamwise direction

DOI: 10.1002/fld

Table II. Comparison of bulk parameters for two different grids: shear parameter $K=0.0$ and 0.4, $L/d=5$ for all the cases. $N_x \times N_y$ refers to number of grid points in the x- and y-directions, respectively.

	Upstream cylinder				Downstream cylinder				
$N_x \times N_y$	$\overline{C}_{\mathrm{L}}$	$\overline{C}_{\mathrm{L,rms}}$	$\overline{C}_{\mathrm{D}}$	$\overline{C}_{\mathrm{D,rms}}$	$\overline{C}_{\mathrm{L}}$	$\overline{C}_{\mathrm{L,rms}}$	$\overline{C}_{\mathrm{D}}$	$\overline{C}_{\mathrm{D,rms}}$	St
$K=0.0$									
469×220	0.000	0.2794	1.423	0.0752	0.014	1.1322	1.089	0.1691	0.137
437×195	0.001	0.2517	1.420	0.0654	0.014	1.0298	1.050	0.3491	0.137
$K=0.4$									
469×220	−0.198	0.1825	0.683	0.0782	−0.128	0.0967	0.434	0.0720	0.053
437×195	−0.211	0.2071	0.681	0.0953	−0.129	0.0961	0.436	0.0738	0.053

Table III. Comparison of bulk parameters for different outlet boundary locations (X_d): shear parameter $K=0.1$ is same for all the cases.

		Upstream cylinder				Downstream cylinder				
L/d	X_d	$\overline{C}_{\mathrm{L}}$	$\overline{C}_{\mathrm{L,rms}}$	$\overline{C}_{\mathrm{D}}$	$\overline{C}_{\mathrm{D,rms}}$	$\overline{C}_{\mathrm{L}}$	$\overline{C}_{\mathrm{L,rms}}$	$\overline{C}_{\mathrm{D}}$	$\overline{C}_{\mathrm{D,rms}}$	St
2	$30d$	0.037	0.0134	1.333	0.0138	−0.065	0.0320	−0.141	0.0133	0.122
2	$20d$	0.038	0.0125	1.332	0.0042	−0.063	0.0294	−0.140	0.0121	0.122
3	$30d$	0.031	0.0032	1.302	0.0164	−0.073	0.0384	−0.109	0.0183	0.114
3	$20d$	0.033	0.0044	1.296	0.0092	−0.079	0.0344	−0.110	0.0159	0.114

is varied. For example, we arrived at a grid size of 386×195 and 471×195 for L/d ratio 2 and 7, respectively.

Further, to investigate the influence of location of the outlet boundary on the results, we have considered two different outlet domain extents *viz.* 20 and 30 times of the cylinder width from the origin. With these extents, we have computed $L/d=2$ and 3 with inlet condition as $K=0.1$. Respective grids arrived at are 386×195 and 418×195. Results obtained from these cases are compared in Table III. The variation of $\overline{C}_{\mathrm{L}}$, $\overline{C}_{\mathrm{D}}$ and St is trivial. However, $C_{\mathrm{L,rms}}$ and $C_{\mathrm{D,rms}}$ values have little difference. From the computational cost point of view, $20d$ is big enough. Hence for the remaining calculations, outlet domain extent of $20d$ has been used. It should be noted that St number for both the cylinders happens to be the same (explained in Section 4.1); hence for only one value is given in both the tables.

4. RESULTS

In this study, numerical simulations were performed for incoming linear shear flow past two equal-sized square cylinders. The cylinders are kept in tandem arrangement. The study includes influence due to variation of shear parameter and gap distance. The shear parameter is varied systematically from 0.0 to 0.4 and the gap distance is varied from 2 to 7. The solution is started with an initial condition, and allowed to march in time up to when it gets stabilized, which is observed from the

DOI: 10.1002/fld

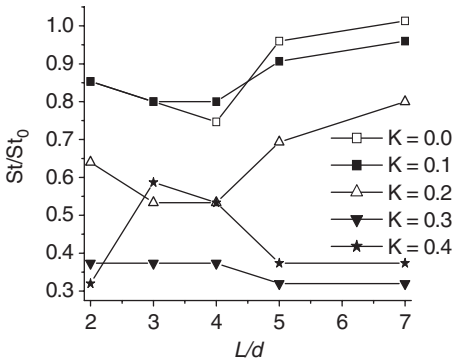

Figure 3. Variation of Strouhal number against the L/d ratio for all shear parameters.

time variation of lift and drag forces. After this, calculations are carried out for over 50 cycles and time averaging is performed. Results in terms of Strouhal number, pressure distribution and vorticity contours are presented and discussed in this section.

4.1. Strouhal number

Figure 3 shows the variation of Strouhal number (St/St_0) with L/d ratio for different values of the shear parameter K. It is obtained from the instantaneous lift signal collected separately for each cylinder over 50 shedding cycles and is normalized by Strouhal number of an isolated square cylinder subjected to without shear (St_0). The instantaneous lift coefficient is defined as $C_L = 2F_L/\rho U^2 A$. It is to be noted that the Strouhal number, St, is identified based on the dominating frequency in the corresponding spectra. The Strouhal number is observed to be the same for both up- and downstream cylinders for any particular combination of L/d and K considered in this study. Similar observation is reported [4] for circular cylinders in tandem arrangement without shear. Hence it is plotted only for one cylinder. For complete understanding of the sub-harmonics, a detailed frequency spectrum is given in Figure 7.

For all the cases considered in this study, the Strouhal number is less when compared with that of isolated square cylinder without shear. Further in interference, except in one case, in all the cases Strouhal number obtained in shear flow is less than that obtained for the same gap distance without shear ($K = 0.0$). Except for L/d ratio 2, with increasing shear, St decreases up to shear parameter 0.3 and then increases. For shear values of $K = 0.0, 0.1, 0.2$, St first decreases up to some L/d ratio and then increases. But for $K = 0.3$, St is constant up to $L/d = 4$, decreases a bit and then remains constant. For $K = 0.4$, St number showed a reverse trend for all L/d ratios except at $L/d = 2$. At $L/d = 3$ and 4, St number is higher than and equal to, respectively, the St at $K = 0.2$ for the same corresponding L/d ratio. This could be due to the concentration of the shedding frequency in a narrow range. When $K = 0.3$, the shedding consists of more than one predominant frequency. Hence St number is lower for $K = 0.3$.

4.2. Coefficient of drag

Figure 4 shows the time-averaged coefficient of drag force ($\overline{C}_D$) normalized by $\overline{C}_{D,0}$ of the isolated square cylinder with uniform inlet flow (i.e. shear parameter $K = 0.0$). Figure 4(a) is for the upstream

DOI: 10.1002/fld

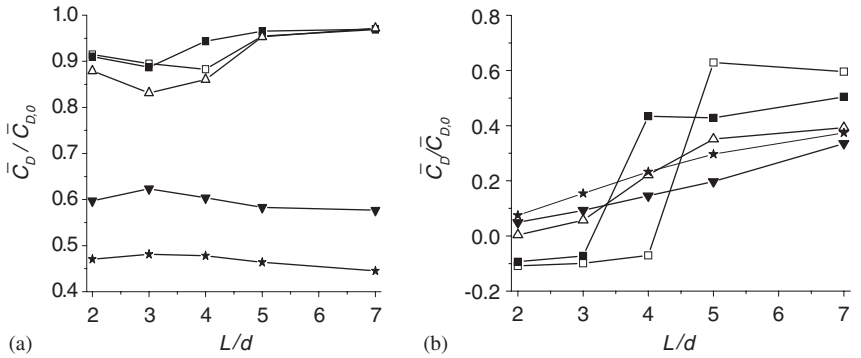

Figure 4. Variation of drag coefficient against the L/d ratio for all shear parameters: (a) upstream cylinder and (b) downstream cylinder. Legends are same as in Figure 3.

cylinder. For low K values (i.e. $0.0, 0.1, 0.2$), the influence of shear on the upstream cylinder drag force is less when compared with that for high K values. When $K=0.0$, $\overline{C}_{\mathrm{D}}$ first decreases up to $L/d=4$ and then increases towards that of the isolated cylinder ($\overline{C}_{\mathrm{D},0}$) with increasing L/d. When $K=0.1$ and 0.2, $\overline{C}_{\mathrm{D}}$ decreases up to $L/d=3$, then increases. With increasing shear, the velocity on the top side of the cylinder is more than that of the bottom side. This leads to the formation region of the vortices behind the cylinders shifting to the bottom side of the cylinder. Further, the difference in the strength of the shear layers coming from the front cylinder becomes more pronounced with increasing K. Owing to that, pressure on the back face of the front cylinder increases. The difference in pressure between the front and back faces, which is nothing but drag force, decreases (see Figure 8). The change in drag curve manifests the onset of vortex shedding from the upstream cylinder. In these cases, it is between $L/d=4$ and 5. With increasing K, this critical gap reduces to between $L/d=3$ and 4. It is very difficult to identify the exact value of L/d for which the onset of shedding occurs for the upstream cylinder as it requires many unsteady simulations.

For $K>0.3$, $\overline{C}_{\mathrm{D}}$ is more or less constant and 40% lower than that of the isolated cylinder. They are less than those observed for $K<0.3$. For the $K=0.4$ case, $\overline{C}_{\mathrm{D}}$ decreases further and becomes almost constant. It is also nearly 50% lower than that of the isolated square cylinder. The influence of L/d on mean drag coefficient when $K>0.2$ is almost insignificant. This might be because the high momentum fluid entering into the gap region of the upstream cylinder felt no influence of the downstream cylinder. Drastic reduction in the mean drag coefficient for high K values could be due to pressure rise on the back face of the front cylinder (see Figure 8).

The $\overline{C}_{\mathrm{D}}$ variation for the downstream cylinder is shown in Figure 4(b). When $K=0.0$, the downstream cylinder experiences a negative drag coefficient up to $L/d=4$. This could be due to the fact that the downstream cylinder is in the low-pressure cavity formed by the separated shear layers from the upstream cylinder. The negative drag coefficient indicates that the cylinders attract each other. This nature is consistent with what is observed in the circular cylinder case studies [4]. The extent is reduced to $L/d=3$, when shear parameter is $K=0.1$. With increasing shear, the high-velocity side shear layer enters into the gap region which disturbs the low-pressure region (cavity region) between the cylinders. Consequently, $\overline{C}_{\mathrm{D}}$ becomes positive for downstream cylinder with increasing shear. For $K>0.2$, $\overline{C}_{\mathrm{D}}$ increased monotonically. For $K=0.3$, $\overline{C}_{\mathrm{D}}$ has a

DOI: 10.1002/fld

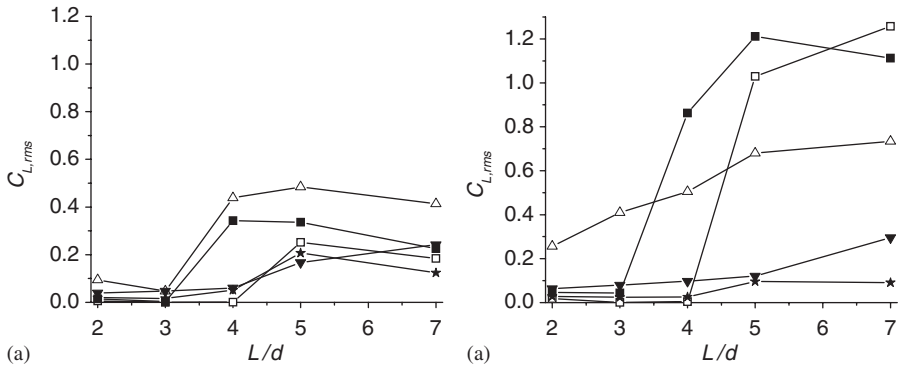

Figure 5. Variation of RMS lift coefficient against the L/d ratio for all shear parameters: (a) upstream cylinder and (b) downstream cylinder. Legends are the same as in Figure 3.

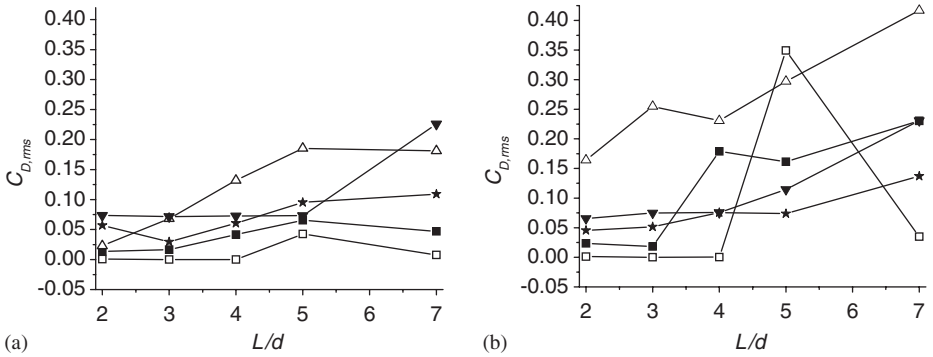

Figure 6. Variation of RMS drag coefficient against the L/d ratio for all shear parameters: (a) upstream cylinder and (b) downstream cylinder. Legends are the same as in Figure 3.

higher value than that of the $K=0.4$ for all L/d considered in this study. This is opposite to the trend noticed in the upstream cylinder. For all the cases, $\overline{C}_{\mathrm{D}}$ is lower than that of the isolated case and corresponding values for upstream cylinder for the same shear.

4.3. RMS values of lift and drag coefficients

The statistical measures of the coefficient of lift and drag variation from the mean value are presented as RMS values. The RMS value is defined as $\sqrt{\sum_{i=1}^{n}(C_{\mathrm{L}}(i)-\overline{C_{\mathrm{L}}})^2/n}$, where C_{L} and $\overline{C_{\mathrm{L}}}$ are the instantaneous and mean lift coefficients, respectively, and n is the total number of discrete points. Figure 5 shows the variation of RMS value of lift coefficient with the L/d ratio for all the shear parameters. At low L/d ratios, $C_{\mathrm{L,rms}}$ is very low. When the upstream cylinder starts to shed vortices, depending on the shear parameter, $C_{\mathrm{L,rms}}$ is increased either after $L/d=3$ or 4. After this L/d ratio, $C_{\mathrm{L,rms}}$ decreases for the upstream cylinder, whereas it continuously increases for the downstream cylinder. However at any particular L/d ratio, with increasing shear, $C_{\mathrm{L,rms}}$ is observed to increase first and decrease later. $C_{\mathrm{L,rms}}$ for the downstream cylinder is always

DOI: 10.1002/fld

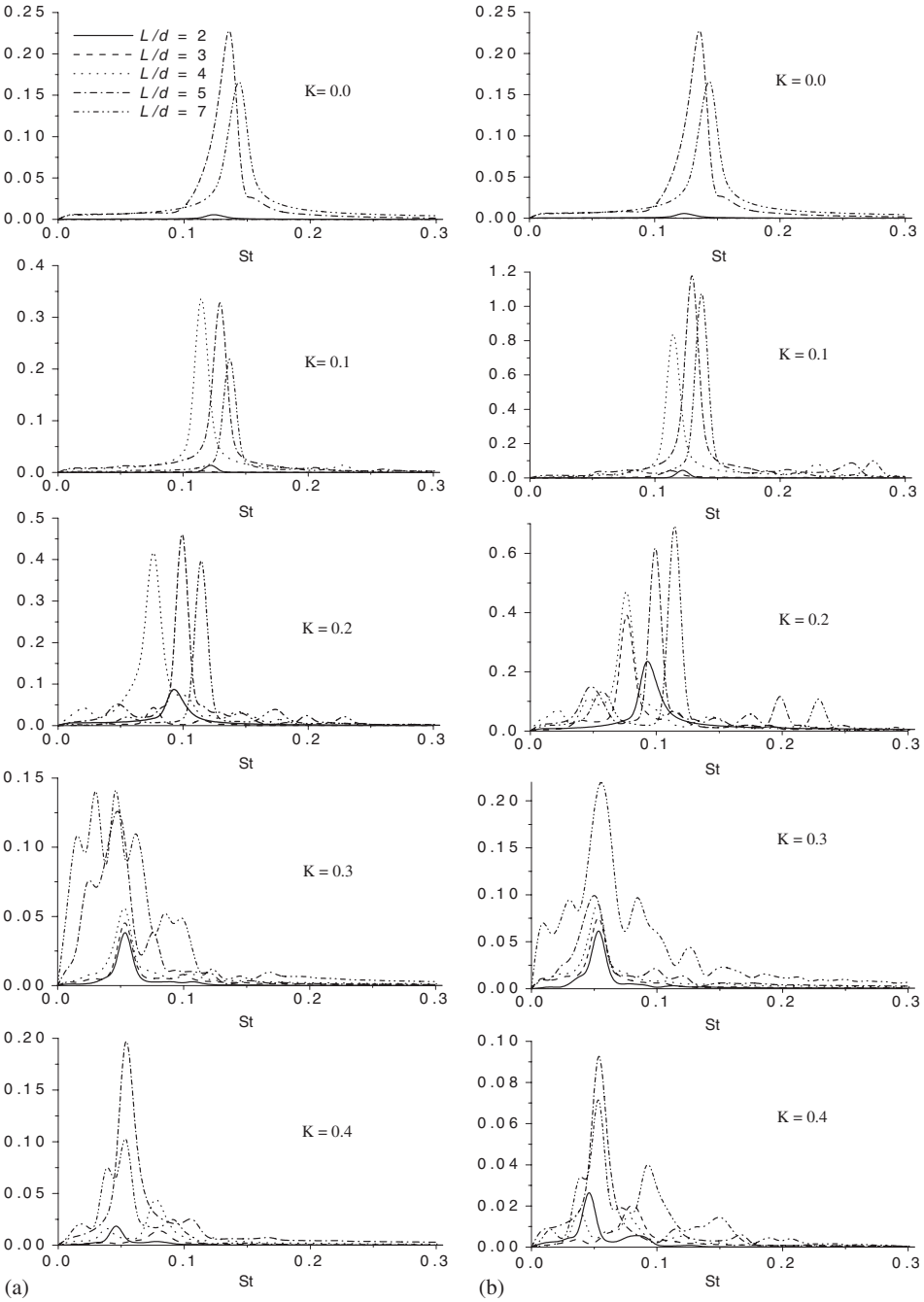

Figure 7. Spectra of the lift coefficient: (a) upstream cylinder and (b) downstream cylinder. Legends are the same for all the plots.

DOI: 10.1002/fld

observed to be higher than that of the upstream cylinder for lower shear parameters and *vice versa* for higher shear parameters.

Variation of RMS value of the drag coefficient is plotted against the L/d ratio for all the shear parameters in Figure 6. $C_{\mathrm{D,rms}}$ increases for both cylinders with increase in L/d ratio. The magnitude of $C_{\mathrm{D,rms}}$ for both cylinders at any particular L/d ratio first increases with increasing shear up to $K=0.2$ and then decreases with increasing shear. For the downstream cylinder, after the critical L/d ratios, the $C_{\mathrm{D,rms}}$ shows increasing trend.

4.4. Spectral analysis

Figure 7 shows the spectra of the time-varying lift coefficient obtained by fast Fourier transform. The sampling rate of the signal is equal to $1/\Delta t$, where Δt is the time step in the numerical simulation. However, only the low and moderate frequencies are explored here as they are closely related to the wake instabilities. The time step used provides a sampling rate much higher than the frequency range of interest; hence, the Nyquest criterion is largely satisfied in this study, preventing aliasing effects. The spectral points considered in this study are 262 144, which gives the spectral resolution of 0.0038. It is recalled that all these magnitudes are expressed in a non-dimensional form. The frequency values read directly from the spectra give the Strouhal number (*St*). The Strouhal number corresponding to the von Karman instability is clearly obtained by the present simulation.

For better clarity, plots are drawn only for important regions. It is also to be noted that the scale on the y-axis is not same in all the plots. For $K=0.0$ and 0.1 and for $L/d=2$, the flow is steady and there is no peak in the spectra. For higher L/d ratios, there is definite peak in the spectra, which gives the predominant non-dimensional shedding frequency called the Strouhal number. This phenomenon is also explained well later with the help of vorticity plots in Figure 9. With increasing K value, the flow becomes complicated. For higher L/d ratios, vortices shedding from the upstream cylinder hit the downstream cylinder and at the same time the downstream cylinder develops its own vortices. These two interact with each other and result in a complicated multifrequency with different values and strength. With increasing K value, the flow separation and reattachment with the downstream cylinder also get altered. For lower L/d ratios, both the cylinders together behave like one cylinder and they get the same single dominant peak in the spectra.

4.5. Coefficient of pressure

The time-averaged coefficient of pressure ($\overline{C}_P$) around the cylinder for all the L/d ratios (L/d) and for all shear parameters K are plotted in Figure 8. In each plot for one particular K value, the effect due to the variation in gap distance is represented. Figure 8(a) is for the upstream cylinder and Figure 8(b) is for the downstream cylinder. It is to be noted that in these plots, in the y-axis, although the actual values are different, the range (that means magnitude of the difference between maximum and minimum values on the y-axis) is the same, separately each for upstream and downstream cylinder. For cylinders, it is observed that with increasing K value and increasing L/d ratio, the stagnation point and the distribution of the time-averaged coefficient of pressure are biased towards the top leading edge. The effect is more pronounced on the downstream cylinder.

The $\overline{C}_P$ distribution on the front face of the upstream cylinder is gradually changed from parabolic to linear pattern with increasing shear irrespective of the L/d ratio. For $K=0$, as expected it behaves like that of the isolated cylinder case. The L/d ratio appears to have insignificant effect

DOI: 10.1002/fld

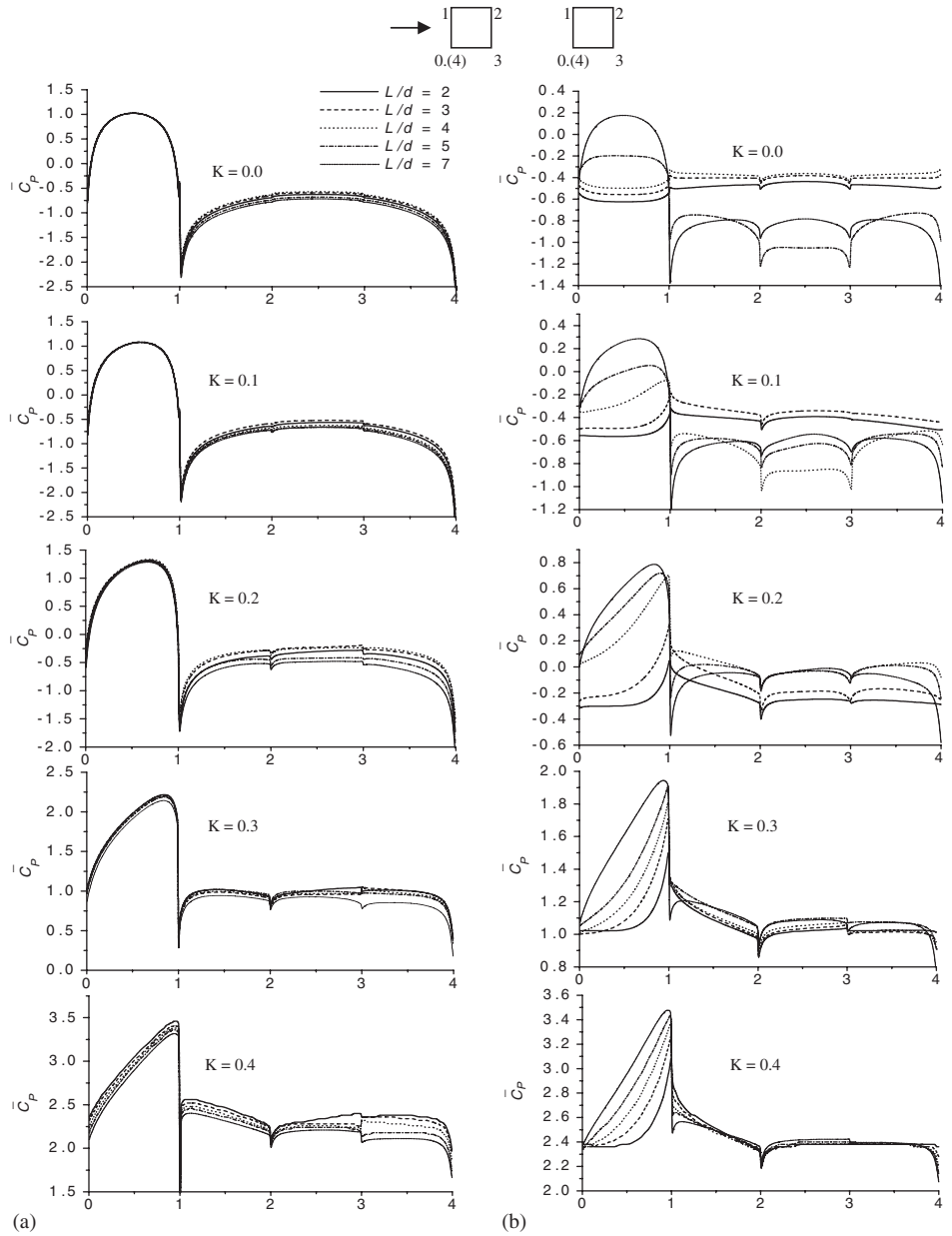

Figure 8. Time-averaged pressure coefficient on the cylinder surface: (a) upstream cylinder and (b) downstream cylinder. Legends are the same for all the plots.

DOI: 10.1002/fld

on the distribution on all the faces in the case of upstream cylinder. This could be due to the fact that the incoming flow does not sense the downstream cylinder as the cylinders are of equal size and placed in tandem arrangement.

On the top and bottom faces of the upstream cylinder, $\overline{C}_P$ distribution is exponentially increased with a minimum value at the leading edge and a maximum at the trailing edge. This variation is due to the flow separation that occurs at the leading edge. At this point, the flow has a maximum velocity due to which $\overline{C}_P$ is low. With increasing K, $\overline{C}_P$ distribution becomes uniform on the top surface. With further increase in K, as we have already seen, stagnation point moves towards the top leading edge; due to that flow accelerates from the leading edge towards the trailing edge. Because of this, $\overline{C}_P$ is decreased from a high value at the leading edge to a lower value at the trailing edge. This is not the case for the bottom face of the upstream cylinder. The $\overline{C}_P$ distribution on the bottom surface follows almost the same trend in all the cases. Interestingly for high K values, $\overline{C}_P$ is positive on all four faces, which means that pressure is always acting towards the cylinder. With increasing shear, velocity on the lower side becomes negative; hence, the flow is in the reverse direction. This reverse flow could increase the wake pressure. The same trend was observed in the literature [3] for high shear values.

The $\overline{C}_P$ distribution on the downstream cylinder front face is strongly affected by the presence of the upstream cylinder. There is also a strong dependence on the L/d ratio. For $L/d \leqslant 4.0$ and $K = 0.0$, the pressure distribution on the front surface of the downstream cylinder is uniform and negative. This could be due to the fact that the shear layers separated from the leading edges of the upstream cylinder develop smoothly over the downstream cylinder. This feature can be observed in Figure 9(a). When $K = 0.0$ and $L/d = 7$, the $\overline{C}_P$ distribution looks like that of the upstream cylinder, though the magnitude is very small. With increasing shear, the stagnation point moves towards the top leading edge. Further, at lower L/d ($\leqslant 4.0$) and for $K \leqslant 0.2$, the $\overline{C}_P$ distribution is different from that of higher L/d values. For $K > 0.2$, the distribution gradually changes from exponential at $L/d = 2$ to linear at $L/d = 7$. This change in the distribution can be attributed to the shift in the stagnation point. With increasing K value, momentum of the shear layer increases. At sufficient L/d ratio, this high momentum fluid accelerates over the front face of the downstream cylinder, whereas at lower L/d ratios, the shear layer glides over the top face of the downstream cylinder. Because of this, $\overline{C}_P$ distribution exponentially varies with a minimum at the bottom leading edge and a maximum at the top leading edge.

When $K = 0.0$ and $L/d \leqslant 4$ and $K = 0.1$ and $L/d \leqslant 3$, the $\overline{C}_P$ distribution is uniform on all the remaining three faces. This trend is attributed to the steady flow. The reason for the steady flow could be due to the following: the downstream cylinder placement could (a) disturb the formation length in the wake of the upstream cylinder, which changes the threshold vorticity at which vortex shedding starts and (b) interrupt the communication between two shear layers of the upstream cylinder. With the increasing shear, the flow becomes unsteady because of which at any particular shear, the $\overline{C}_P$ distribution decreases as L/d ratio increases. It is also observed that on the top face, the $\overline{C}_P$ distribution is strongly affected by the shear flow when compared with that on the bottom face.

4.6. Instantaneous vorticity contours

In order to understand the development of the flow in a better way, instantaneous vorticity contours are plotted in Figure 9. In all the plots, vorticity is plotted at the instant corresponding to the maximum in the respective lift cycle.

DOI: 10.1002/fld

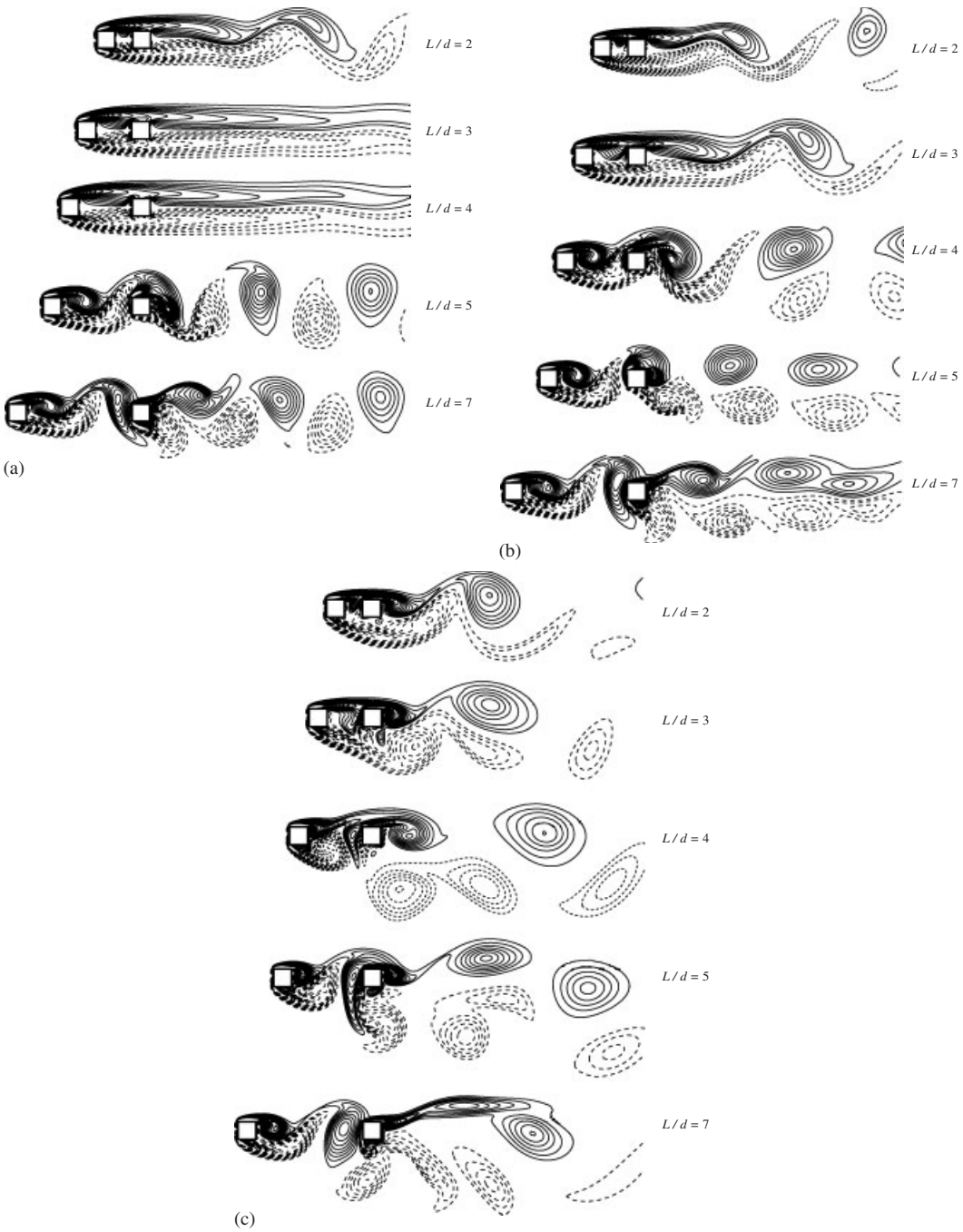

Figure 9. Instantaneous vorticity contours for all L/d ratios: (a) $K=0.0$; (b) $K=0.1$; and (c) $K=0.2$. Maximum and minimum vorticity are set at 4.0 and -4.0, respectively, in steps of 0.2. Solid line is for positive vorticity and dashed line is for negative vorticity.

DOI: 10.1002/fld

Figure 9(a) shows the instantaneous vorticity contours for $K=0.0$. When $L/d=2$, the flow becomes unsteady in the far wake. For $L/d=3$ and 4, the flow is steady. With further increase in L/d, the flow again becomes unsteady throughout the wake. At high L/d ratios, there is a definite wake behind the upstream cylinder and alternate vortex shedding, which is trapped in the gap between the cylinders. When $L/d=5$, due to lack of sufficient gap between the cylinders, the vortical structure touches the downstream cylinder before its complete evolution. When $L/d=7$, there is sufficient gap for the vortices to develop; hence, they are completely developed before hitting the downstream cylinder. The vortical structures in the wake of downstream cylinder are closely spaced when compared with those for the lesser L/d ratios and they have the typical vortex shape.

Figure 9(b) shows the instantaneous vorticity contours at $K=0.1$ for different L/d ratios. Up to $L/d=3$ the flow exhibits unsteady behavior in the far wake only. With increasing L/d ratio, the flow becomes completely unsteady. The upstream cylinder is able to develop its own wake behind it. The vortex developing from the upstream cylinder hits the downstream cylinder. Because of that the instantaneous stagnation point keeps oscillating. Owing to the continuous movement of the stagnation point, the wake structure for the downstream cylinder is also altered. When $L/d=5$, the stagnation point on the downstream cylinder is at the bottom corner. However, when $L/d=7$, the stagnation point has moved to the top corner. For the upstream cylinder, vortices shed in an alternate fashion. After hitting the downstream cylinder, they shed simultaneously. This is due to the fact that structure coming from upstream cylinder hits the downstream cylinder, then breaks down into two parts and then passes over the two sides of the downstream cylinder. The convective velocity of the structures decreases downstream. Consequently in the far field two adjacent vortices with same sign pair with each other and finally they are amalgamated into one structure. After this process, vortices are observed to shed in an alternate fashion. However, the strength of the negative sign vortices is very weak and one can expect the flow to be dominated by the clockwise vortices further downstream. Williamson [29] had defined elliptic and circular vortices based on the ratio of strain to the vorticity. Elliptic flow ensues if the ratio is in between 0 and 1. Circular rotating flow refers to zero strain (i.e. ratio between strain to vorticity is zero). In the present cases, the vortices downstream appear in either elliptic or circular (round) shape. Elliptic vortices from the upstream cylinder pass over the downstream cylinder; they become almost round. This implies that flow is dominated by the vorticity rather than strain rate. Again after coalescence downstream, they become elliptic.

Figure 9(c) shows the instantaneous vorticity when $K=0.2$ for all L/d ratios. It is observed that the flow is unsteady for all L/d ratios. When $L/d=2$, the flow behaves like flow past a single cylinder. Shear layers coming from the upstream cylinder are biased towards the lower velocity side due to shear. Because of this, the shear layer coming from the higher velocity side of the upstream cylinder hits the top portion of the front face of the downstream cylinder. The flow accelerates from here and develops with negative vorticity on the front face of the downstream cylinder. This flow breaks the shear layer embedded with positive vorticity coming from the upstream cylinder. Because of this, we observe a small pocket of positive vorticity trapped between negative vortices, flowing near the bottom side of downstream cylinder. When $L/d=7$, the flow is very complex behind the downstream cylinder. There are multiple structures. Owing to shear, negative vortices from the upstream cylinder do not hit the downstream cylinder; they just pass beneath the downstream cylinder. Because of that, in the near wake of the downstream cylinder, both positive and negative vortices are shed separately and also the number of negative vortices is more when compared with the positive vortices.

DOI: 10.1002/fld

The phase difference between the upstream and downstream cylinder shedding varies with the L/d ratio. There is nearly 180° phase difference between the cylinders at $L/d=7$ irrespective of the inlet shear. However, when $L/d<7$, shedding is observed to be with small phase difference.

5. CONCLUSIONS

In this study, the flow past a pair of square cylinders of equal size in tandem arrangement in uniform shear was considered to investigate the effect of inlet shear rate and L/d ratio between the cylinders. The Reynolds number considered was $Re=100$. The inlet shear rates considered were $K=0.0$–0.4 in steps of 0.1 and the L/d ratio was varied from 2 to 7.

Vortex shedding frequency was decreased with increasing shear rate and also for all the cases considered in this study, it was observed to be less when compared with that of an isolated cylinder. At higher L/d ratios and shear rates, there was more than one dominating frequency.

The upstream cylinder mean drag coefficient $\overline{C}_{\mathrm{D}}$ showed a decreasing trend with increasing shear rate for all the L/d ratios except for $L/d=4$ and 5, when $K=0.1$. In the downstream cylinder the variation of $\overline{C}_{\mathrm{D}}$ with shear and L/d ratio showed a mixed trend, but lower than that of the upstream cylinder and far lower than that of the single cylinder with $K=0.0$. At lower L/d ratios and at shear rates of $K=0.0$ and 0.1, the downstream cylinder experienced negative $\overline{C}_{\mathrm{D}}$. With increasing K value, $\overline{C}_{\mathrm{D}}$ has moved to the positive side. For all values of the shear parameter, the RMS values of both lift and drag coefficient were higher for the downstream cylinder. With increasing L/d ratio, RMS values changed for both lift and drag.

With increasing shear parameter ($K>0.0$), the time-averaged coefficient of pressure $\overline{C}_P$ on the front face of both the cylinders was gradually changed to a linear distribution with stagnation point at the top leading edge. However for $K=0.0$, the $\overline{C}_P$ distribution was parabolic with the stagnation point at the center of the front face. However, the instantaneous stagnation point was oscillating on the front face of the downstream cylinder. The magnitude of $\overline{C}_P$ was quite a bit lower in case of the downstream cylinder compared with the upstream one. Both cylinders experienced positive $\overline{C}_P$ distribution on the four faces, when $K>0.2$.

When $K=0.0$ and 0.1 the flow was steady up to $L/d=4$ and 3, respectively. It can be observed that with increasing shear parameter, the flow becomes unsteady much earlier i.e. at lesser L/d ratio, compared with the uniform flow case. There was a definite wake behind the upstream cylinder when $L/d>4$. At $L/d<4$, even though the flow was unsteady for some combinations of L/d and K, there was no definite wake for the upstream cylinder. When the L/d ratio was higher, the influence of upstream cylinder on the downstream cylinder vortex evolution was more. There was parallel vortex shedding behind the downstream cylinder for higher K and L/d values. In the far wake, the flow is dominated by the clockwise vortices.

ACKNOWLEDGEMENTS

The authors are grateful to the referees for their valuable comments that helped to improve the quality of the paper.

REFERENCES

1. Noda H, Nakayama A. Free-stream turbulence effects on the instantaneous pressure and forces on cylinder of rectangular cross section. *Experiments in Fluids* 2003; **34**:332–344.

DOI: 10.1002/fld

2. Cheng M, Tan SHN, Hung KC. Linear shear flow over a square cylinder at low Reynolds number. *Physics of Fluids* 2005; **17**:078103.
3. Cheng M, Whyte DS, Lou J. Numerical simulation of flow around a square cylinder in uniform-shear flow. *Journal of Fluids and Structures* 2007; **23**:207–226.
4. Mittal S, Kumar V, Raghuvanshi A. Unsteady incompressible flows past two cylinders in tandem and staggered arrangements. *International Journal for Numerical Methods in Fluids* 1997; **25**:1315–1344.
5. Papaioannou GV, Yue DKP, Triantafyllou MS, Karniadakis GE. Three-dimensionality effects in flow around two tandem cylinders. *Journal of Fluid Mechanics* 2006; **558**:387–413.
6. Zdravkovich MM. Review of flow interference between two circular cylinders in various arrangements. *Journal of Fluids Engineering* (ASME) 1977; **99**:618–633.
7. Zdravkovich MM. The effect of interference between circular cylinders in cross flow. *Journal of Fluids and Structures* 1987; **1**:239–261.
8. Sakamoto H, Haniu H, Obata Y. Fluctuating forces acting on two square prisms in a tandem arrangement. *Journal of Wind Engineering and Industrial Aerodynamics* 1987; **26**:85–103.
9. Meneghini JR, Saltara F, Siqueira CLR, Ferrarijr JA. Numerical simulation of flow interference between two circular cylinders in tandem and side-by-side arrangements. *Journal of Fluids and Structures* 2001; **15**:327–350.
10. Carmo BS, Meneghini JR. Numerical investigation of the flow around two circular cylinders in tandem. *Journal of Fluids and Structures* 2006; **22**:979–988.
11. Deng J, Ren AL, Zou JF, Shao XM. Three-dimensional flow around two circular cylinders in tandem arrangement. *Fluid Dynamics Research* 2006; **38**:386–404.
12. Jordan SK, Fromm JE. Laminar flow past a circle in a shear flow. *Physics of Fluids* 1972; **69**:972–979.
13. Kiya M, Tamura H, Arie M. Vortex shedding from a circular cylinder in moderate Reynolds number shear flow. *Journal of Fluid Mechanics* 1980; **101**:721–735.
14. Kwon S, Sung HJ, Hyun JM. Experimental investigation of uniform shear flow past a circular cylinder. *Journal of Fluids Engineering* (ASME) 1992; **114**:457–460.
15. Mukhopadhyay A, Venugopal P, Vanka SP. Numerical study of vortex shedding from a circular cylinder in linear shear flow. *Journal of Fluids Engineering* (ASME) 1999; **121**:460–468.
16. Xu Y, Dalton C. Computation of force on a cylinder in a shear flow. *Journal of Fluids and Structures* 2001; **15**:941–954.
17. Sumner D, Akosile OO. On uniform planar shear flow around a circular cylinder at sub-critical Reynolds number. *Journal of Fluids and Structures* 2003; **18**:441–454.
18. Ayukawa K, Ochi J, Kawahara G, Hirao T. Effect of shear rate on the flow around a square cylinder in a uniform shear flow. *Journal of Wind Engineering and Industrial Aerodynamics* 1993; **50**:97–106.
19. Hwang RR, Sue YC. Numerical simulation of shear effect on vortex shedding behind a square cylinder. *International Journal for Numerical Methods in Fluids* 1997; **25**:1409–1420.
20. Saha AK, Muralidhar K, Biswas G. Numerical study of the turbulent unsteady wake behind a partially enclosed square cylinder using RANS. *Computer Methods in Applied Mechanics and Engineering* 1999; **178**:323–341.
21. Saha AK, Biswas G, Muralidhar K. Two-dimensional study of the turbulent wake behind a square cylinder subject to uniform shear. *Journal of Fluids Engineering* 2001; **123**:595–603.
22. Sohankar A, Norberg C, Davidson L. Simulation of three-dimensional flow around a square cylinder at moderate Reynolds number. *Physics of Fluids* 1999; **11**:288–306.
23. Hirt CW, Cook JL. Calculating three-dimensional flow around structures and over rough terrain. *Journal of Computational Physics* 1972; **10**:324–340.
24. Nakayama A, Vengadesan SN. On the influence of numerical schemes and subgrid stress models on LES of turbulent flow past a square cylinder. *International Journal for Numerical Methods in Fluids* 2002; **38**:227–253.
25. Kumaran M, Vengadesan S. Flow characteristics behind rectangular cylinders placed near a wall. *Numerical Heat Transfer—Part A* 2007; **52**:643–660.
26. Kurosey R, Komori S. Drag and lift forces on a rotating sphere in a linear shear flow. *Journal of Fluid Mechanics* 1999; **384**:183–206.
27. Lankadasu A, Vengadesan S. Numerical simulation of flow over a square cylinder with linear shear. *Proceedings of the 33rd National and 3rd International Conference on Fluid Mechanics and Fluid Power*, IIT Bombay, India, December 2006.
28. Okajima A. Strouhal number of rectangular cylinders. *Journal of Fluid Mechanics* 1982; **123**:379–398.
29. Williamson CHK. Three-dimensional wake transition. *Journal of Fluid Mechanics* 1996; **328**:345–407.

DOI: 10.1002/fld